

Individual addressing of trapped ions and coupling of motional and spin states using rf radiation

M. Johanning,¹ A. Braun,¹ N. Timoney,¹ V. Elman,¹ W. Neuhauser,² and Chr. Wunderlich¹

¹Fachbereich Physik, Universität Siegen, 57068 Siegen, Germany

²Institut für Laser-Physik, Universität Hamburg, Luruper Chaussee 149, 22761 Hamburg, Germany

(Dated: April 23, 2022)

We demonstrate for the first time two essential experimental steps towards realizing a novel concept for implementing quantum computing, quantum simulations and creating large entangled states of individually accessible subsystems - an ion spin molecule: Trapped atomic ions are individually addressed in frequency space using rf-radiation. In addition, an interaction between motional and spin states induced by a static magnetic field gradient is demonstrated.

Quantum computations and simulations are expected to yield new insight into as of yet unsolved physical problems that withstand efficient treatment on a classical computer (e.g., [1, 2, 3, 4]). Already a small number of qubits (i.e., a few tens) used for quantum *simulations* can solve problems even beyond the realm of quantum information science. Creating and investigating entanglement in large physical systems is a related important experimental challenge with implications for our understanding of the transition between the elusive quantum regime and the classical world [5, 6].

A central goal in the interdisciplinary research field of quantum information processing (QIP) is the realization of universal quantum computation, and basic ingredients for a QC have indeed been demonstrated in various experimental systems [7]. Also, laser cooled atomic ions confined in an electrodynamic cage have successfully been used for QIP [8, 9, 10, 11] and advantages and drawbacks of this system have been investigated in great detail. Each experimental systems has specific advantages and difficulties when it comes to scaling up these successful demonstrations to a large number of qubits such that universal fault-tolerant quantum computing is achieved.

For instance, concepts for a scalable universal ion trap quantum computer (ITQC) [12] rely on conditional quantum dynamics with two qubits at a time, thus making necessary physical transport of ions between storage and interaction regions. Restricting quantum gates to two qubits is mostly rooted in the fact that individual addressing of N ions (with $N \gg 1$) is difficult when employing, for instance, two laser beams that are supposed to induce Raman transitions (and thus are not collinear) in one particular ion embedded in a long ion string. Also, cooling N axial vibrational modes of an ion string composed of N ions close to their motional ground state is time consuming and may be difficult.

However, using more than two ions at a time for conditional quantum dynamics (i.e., performing multi-qubit gates) can considerably reduce the computational time needed for executing a given quantum algorithm in two ways: i) Decomposing a quantum algorithm for execution on a physical device into N -qubit gates ($N > 2$) instead of 2-qubit gates can give a speed-up that increases with N [13, 14]. ii) The time needed for physically moving ions is strongly reduced.

Performing multi-qubit gates requires coupling of several ions which is given when employing an ion spin molecule [15, 16, 17]. The term ion spin "molecule" is used here to de-

scribe a Coulomb crystal of atomic ions exposed to a magnetic field gradient that induces pairwise coupling J_{ij} between the internal qubit states (spins) of ion i and j ($i, j = 1, 2, 3, \dots, N$ with N the number of ions, see below). This term is employed referring to a pseudomolecule [18] whose constituents exhibit a physical interaction with a mathematical description identical to J -coupling in molecules. However, here the coupling constants between spins are adjustable. Also, this artificial molecule is well isolated from its environment. In addition, individual addressing of spins in frequency space instead of position space is possible with ion spin molecules, even for strings of several tens of ions [19]. Thermal excitation of vibrational motion typically at the Doppler limit is expected not to impede quantum logic gates [20]. An ITQC based on ion spin molecules may be realized by using a similar array of ion traps as proposed in [12], but with many qubits in one interaction region coupled by local field gradients, thus allowing for a speed-up of quantum algorithms.

If considering N trapped ions that form a Coulomb crystal and are exposed to a spatially varying magnetic field gradient, then the following coupling Hamiltonian arises [15, 16, 19]

$$H_I = -\frac{\hbar}{2} \sum_{i < j}^N J_{ij} \sigma_{z,i} \sigma_{z,j}. \quad (1)$$

Here, the Pauli matrices σ_z describe two suitably chosen internal states of each ion (a spin-1/2, \hbar is Planck's constant divided by 2π). The coupling constants for N ions are given by

$$J_{ij} = \sum_{n=1}^N v_n \kappa_{ni} \kappa_{nj} \quad (2)$$

where

$$\kappa_{nl} = S_{nl} \frac{\partial_z \omega_l \Delta z_n}{v_n} \quad (3)$$

measures the coupling of spin l to the n -th vibrational mode of the ion string (Δz_n is the extension of the ground state wavefunction of the n -th vibrational mode, v_n the angular frequency that characterizes this mode, and S_{nl} is the relative excursion of ion l when taking part in mode n). This coupling is induced by the non-vanishing spatial derivative $\partial_z \omega_l$ of the transition frequency of qubit l . The magnitude of the coupling constants J_{ij} can be adjusted by varying the magnetic field gradient and the trap frequency ν_l . The range of

the coupling may be determined by using additional dc trap electrodes [17].

Quantum *simulations* relax experimental requirements considerably, since highly accurate local control over qubit dynamics, as required for a circuit model-based QC can often be replaced by globally controlling the qubit interactions. In addition, one expects to be able to tackle useful applications already with a moderate number of qubits. With so-called Hamiltonian simulation universal QC can be implemented while a more restricted quantum simulator is able to address specific physics problems. An ion spin molecule is useful in this respect, since spin chains with globally and locally adjustable coupling parameters can be realized and are well suited, for instance, for simulating magnetism of quantum systems [3, 21]. Also, an ion spin molecule is well suited to implement a classical neural network or error-resistant quantum computing based on a quantum neural network [22, 23].

Characterizing multi-partite entanglement, its consequences and implications for many physical phenomena, and the role of entanglement in the transition from the quantum to the classical world is a central research theme not only in quantum information science. Thus experimentally creating and efficiently analyzing entangled states with a large and controlled number of subsystems (e.g., qubits) is an important challenge. An ion spin molecule will allow for the well controlled creation of entangled states composed of a large number of qubits. For instance, large two-dimensional cluster states [24, 25] can be efficiently generated [26].

The experiments presented here were performed with laser cooled $^{172}\text{Yb}^+$ -ions in a linear Paul trap. A detailed description of the trap and the experimental set-up can be found in [27].

The metastable $D_{3/2}$ -state (lifetime of 52.2 ms [28]) plays an important role in the experiments presented here. Individual addressing of ions and the coupling between motional and internal ionic states is demonstrated using rf-optical double resonance spectroscopy on this state. The degeneracy of its Zeeman-manifold is lifted by a magnetic field $B = B_0 + z \partial_z B$ composed of an offset field B_0 and an additional field with constant gradient $\partial_z B$ (z is the axis of rotational symmetry of the trapping potential and thus of the linear ion string). The magnitude of B determines the resonance frequency of magnetic dipole transitions between the Zeeman states. The (linear) Zeeman shift ΔE_J by a magnetic field B is given by $\Delta E_J = g_J m_J \mu_B B$ with Landé g-factor g_J , magnetic quantum number m_J , and the Bohr magneton μ_B . Magnetic dipole transitions between levels with $\Delta m_J = \pm 1$ with resonance frequency

$$f = \frac{g_J \mu_B B}{h} \quad (4)$$

are driven using an rf field that is generated by a dipole coil. The magnitude of B_0 was chosen for most experiments to be about 0.67 mT resulting in a resonance frequency $f \approx 7.5$ MHz.

This four level system is initialized by optical pumping: a laser light field near 935 nm (labeled "repumper" in what follows) with its linear polarization aligned parallel to \vec{B} allows

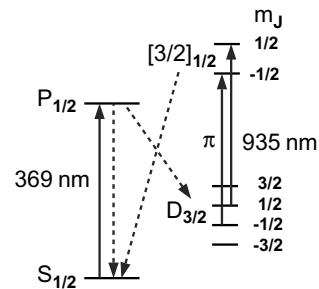


FIG. 1: Scheme of the relevant energy levels of $^{172}\text{Yb}^+$ (not to scale). The electric dipole transition between the $S_{1/2}$ ground state and the $P_{1/2}$ excited state near 369 nm is used for Doppler cooling and state selective detection by detecting resonance fluorescence with a photomultiplier or an intensified CCD camera ("cooling fluorescence"). Laser light near 935 nm coupling the metastable state $D_{3/2}$ -state to the $[3/2]_{1/2}$ state allows for control of optical pumping into the $D_{3/2}$ -state.

π -transitions ($\Delta m = 0$) only (see figure 1). Since repumping occurs through the state $[3/2]_{1/2}$ with $m = \pm 1/2$, population accumulates in the "dark" $m = \pm 3/2$ states, and in turn the resonance fluorescence near 369 nm stops. Upon coupling the Zeeman sublevels with a resonant rf field the resonance fluorescence reappears. Modelling the ionic dynamics in the stationary state using rate equations shows the intensity of scattered light near 369 nm to be proportional to the population in the $D_{3/2}$ Zeeman states with $m = \pm 1/2$.

Figure 2 displays results of rf-optical double resonance spectroscopy with an offset field B_0 only (i.e., $\partial_z B = 0$). The coherent temporal evolution of the four Zeeman states driven by the rf field is made irreversible by resonantly coupling it to the spontaneously decaying $[3/2]_{1/2}$ state by the repumper (laser light and rf fields are both on during the measurement). The Rabi frequencies characterizing both the rf and the repumping transition, contribute to the width of the spectrum and can be extracted from Lorentzian fits to the spectra when both are varied experimentally. For this purpose the four-level dynamics are numerically simulated using optical Bloch equations. Here effective decay rates of the Zeeman states $m = \pm 1/2$ are introduced due to their coupling to the $[3/2]_{1/2}$ state by the repumper and subsequent spontaneous decay either directly back to the $D_{3/2}$ Zeeman manifold or to the $S_{1/2}$ state. Population in the $S_{1/2}$ state in turn is excited by the cooling laser and repopulates the $D_{3/2}$ Zeeman states. The predominant decay through the electronic states $S_{1/2}$ and $P_{1/2}$ and the direct decay back to the $D_{3/2}$ are found to repopulate all Zeeman levels equally.

Addressing of individual ions is achieved without focussing the radiation down to less than the spatial separation of adjacent ions by now applying a spatially varying magnetic field $B = B_0 + z \partial_z B$ such that the Zeeman shift is different for each ion. The frequency separation of the resonances of two neighboring ions is given by

$$\Delta f = \frac{g_J \mu_B \delta z \partial_z B}{h} \quad (5)$$

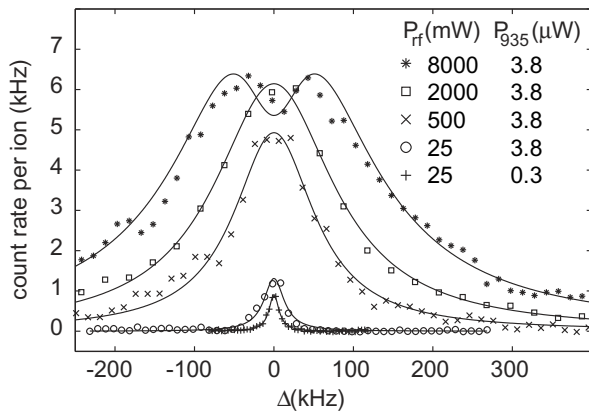


FIG. 2: Resonance fluorescence near 369 nm as a function of the detuning Δ of the rf radiation driving transitions between the Zeeman states of the $D_{3/2}$ -state in $^{172}\text{Yb}^+$ without magnetic field gradient ($\Delta \equiv f_{rf} - f_0$ where f_0 is the ionic resonance frequency and f_{rf} the frequency of the applied rf radiation). The linewidth is determined by the intensity of both, the rf radiation and the laser light near 935 nm (repumper). Here, linewidths between 15 kHz and 310 kHz are observed for rf powers between 25 mW and 8 W and repumping powers between .3 and 3.8 μW focussed to a spot size of approximately 100 μm in diameter. These data were taken with ion strings composed of 4 to 14 ions.

with ion separation δz . The inhomogeneous field along the trap axis is created by cylindrical Nd-permanent-magnets with a diameter of 30 mm in quadrupole configuration separated by approximately 12 cm. The magnetic flux density at the surface of the permanent magnets exceeds 1 T.

The resonance fluorescence spectra in figure 3 demonstrate individual addressing of strings of up to three ions. These spectra exhibit well resolved peaks each corresponding to a resonance of an individual trapped ion. Upon selecting the rf frequency, selective repumping of just one particular ion that fulfills the resonance condition occurs, that is, it scatters resonance fluorescence while the other ions remain dark. When scanning the rf frequency, one ion after the other comes into resonance and consequently scatters light. The data shown in figure 3 illustrate that the ions can be clearly resolved.

The axial trap frequency was measured by parametric heating to be 36.3(5) kHz, yielding ion separations of 31.7(3) μm for two ions and 25.0(2) μm for three ions, respectively. (The radial trap frequency was ≈ 600 kHz.) The experimentally determined frequency separation of the ionic resonances (figure 3) together with equation (5) yield the magnitude of the field gradient $\partial_z B = 0.27(1)$ T/m. The maximum gradient observed was 0.51(2) T/m. Thus frequency separations of up to 130 kHz could be achieved, and with a line width of 15 kHz, unwanted excitation of vicinal ions is reduced to below 0.4 %.

To resolve individual ionic resonances with low cross talk, the Rabi frequency of the rf transition has to be smaller than the frequency separation of Zeeman resonances of vicinal ions. Thus for higher Rabi frequencies (and consequently faster gate operations) the field gradient must be increased. When increasing the number of ions in a linear trap, their spa-

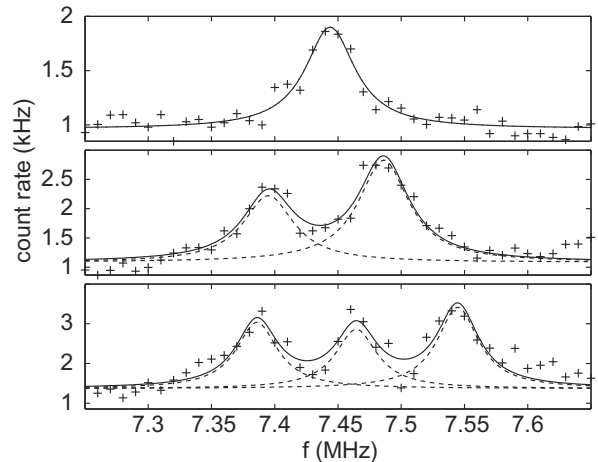


FIG. 3: Individual addressing in frequency space of one (top), two (middle) and three (bottom) trapped ions, respectively. The frequency separation between neighboring ions is extracted by fitting a sum of Lorentzian line profiles and is 91(3) kHz for two ions and 79(4) kHz (middle-left) and 80(4) kHz (middle-right) for three ions. The average ratio of these frequency separations is 1.15(7) which is in good agreement with the analytical prediction of $\sqrt[3]{8/5} \approx 1.17$ for a constant gradient. Together with the extracted FWHM of 49(5) kHz the spurious excitation of adjacent ions is 6.7(8) % in the case of two ions.

tial separation decreases, again making necessary an increasing field gradient to separate neighboring resonances.

If N ions are to be distinguished in frequency space, then a magnetic field gradient

$$\partial_z B \geq \frac{\hbar}{2\mu_B} \left(\frac{4\pi\epsilon_0 m}{e^2} \right)^{\frac{1}{3}} v_1^{\frac{5}{3}} \left(4.7N^{0.56} + 0.5N^{1.56} \right) \quad (6)$$

is needed [19], assuming a linear Zeeman shift as is the case in the experiments presented here. Here, ϵ_0 is the dielectric constant of the vacuum, e represents the elementary charge, and m is the mass of one ion. Using microstructured ion traps, gradients up to 100 T/m are expected, thus making about 40 Yb ions distinguishable in frequency space at a trap frequency of $2\pi \times 260$ kHz.

Figure 4 is composed of spatially resolved images showing a string of four ions taken with an intensified CCD camera while setting the rf frequency to specific values that correspond to individual ionic resonances. It demonstrates that the peaks of the resonance fluorescence observed in figure 3 indeed originate from different ions. Moreover, it shows that single ions are selectively repumped by setting the rf frequency to a particular individual ionic resonance. Here, the spatial separation of the outer ions is 61.3 μm (trap frequency of $2\pi \times 46$ kHz). Using equation (5) this yields a gradient of 0.24 T/m for this experiment.

When a trapped ion interacts with electromagnetic radiation, this may not only affect the atom's internal state but also its motional state. If the line width of a transition between internal states is much smaller than the trap frequency (strong

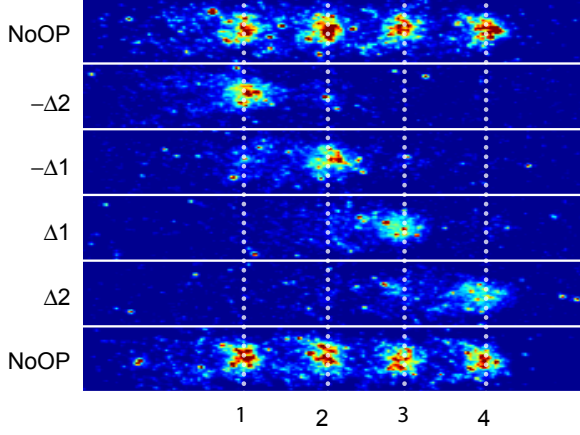


FIG. 4: Individually addressing a single ^{172}Yb ion that is part of a linear Coulomb crystal composed of four ^{172}Yb ions. Four images of the same ion string are shown. These were taken successively from top to bottom. The uppermost and lowermost image labeled 'NoOP' are recorded with no optical pumping, that is, all ions scatter light. For the intermediate pictures, the magnetic field direction is rotated to coincide with the polarization of the repumper, allowing optical pumping. In addition, the rf frequency was set to the expected resonance of one particular ion. Thus, all ions except one remain dark. The detuning $\Delta 1$ or $\Delta 2$ of the rf frequency necessary to address a desired ion is indicated on the left-hand-side of the graph and is given relative to the Zeeman resonance of a single ion. This single-ion resonance was determined before trapping four ions. Here, the detuning $\Delta 1 = 26.3$ kHz and $\Delta 2 = 83.2$ kHz was used. These values are calculated using the number of ions trapped and the frequency separation of two ions measured beforehand.

trapping), motional sidebands accompany this resonance [29]. Such a sideband in the ionic spectrum is due to the coupling between internal and motional dynamics of the ion. This coupling is exploited in ion traps to realize conditional quantum dynamics, for instance, a CNOT gate [8, 30, 31]. The Lamb-Dicke parameter η – the square root of the ratio between the recoil energy and harmonic oscillator energy for an angular trap frequency ν_l – determines its strength:

$$\eta = \sqrt{\hbar^2 k^2 / 2m\hbar\nu_l}. \quad (7)$$

Here, the wave number $k = 2\pi/\lambda$ (λ is the wavelength of the radiation exciting the ion) and thus η is negligibly small when using rf or microwave radiation in contrast to optical photons. For the interaction in an inhomogeneous magnetic field, however, the Zeeman energy and thus the ion's equilibrium position may become state dependent. Therefore, when changing the internal state, the ion will oscillate around its new equilibrium position as if it had received a momentum kick (in a classical picture) [16]. The coupling of internal and motional state is now described by an *effective* Lamb-Dicke parameter η_{eff} that (for a single ion), is given by the ratio between the frequency change of the resonance over the spatial extension $\Delta z = \sqrt{\hbar/2m\nu_l}$ of the ion's wavefunction and the

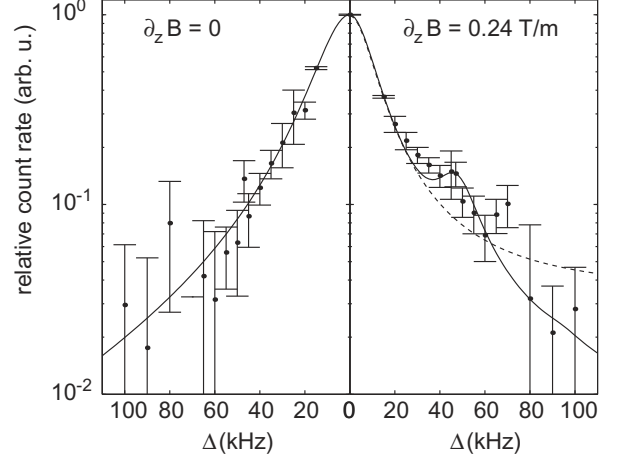


FIG. 5: Comparison of two spectra with improved signal-to-noise ratio recorded with a single ion exposed to a magnetic field gradient (right-hand side) and without field gradient (left-hand side), respectively. The solid line represents a fit using two Lorentzian lines (rhs) or a single Lorentzian (lhs and dashed line on the rhs). The motional sideband accompanying the spin resonance signifies coupling between spin degrees of freedom and the motion of the trapped Yb^+ ion.

trap frequency [19]:

$$|\eta_{\text{eff}}| = \sqrt{\eta^2 + \kappa^2} \approx |\kappa| = \left| \frac{\Delta z \partial_z \omega_{\text{rf}}}{\nu_l} \right| \quad (8)$$

Here, the experimentally determined parameters for the magnetic field gradient and trap frequency yield $\eta_{\text{eff}} = 1.1 \cdot 10^{-3}$.

Neglecting saturation, the amplitudes of the lower and upper motional sidebands have a relative height compared to the carrier given by

$$\frac{a_l}{a_0} = \langle n \rangle \eta_{\text{eff}}^2 \quad \text{and} \quad \frac{a_u}{a_0} = (\langle n \rangle + 1) \eta_{\text{eff}}^2 \quad (9)$$

with $\langle n \rangle$ being the mean phonon number [29], and for large $\langle n \rangle$ we have $a_l \approx a_u \equiv a_s$.

A comparison of two rf-optical double resonance spectra taken with single ions with and without magnetic field gradient, respectively is shown in figure 5. The spectra shown in figure 5 differ only in the magnetic field B applied to the ion: B is homogeneous for the left spectrum (i.e. $\partial_z B_1 = 0$ and thus $\eta_{\text{eff}} = 0$), while a field gradient is applied for the right spectrum. The measurement procedure is in principle as detailed above, with alternating rf optical double resonance and cooling cycles. However, in order to resolve the motional sideband with sufficient signal-to-noise ratio additional measures have been taken: CCD images are taken simultaneously with the rf scans and, preceding each measurement, a fast rf scan through the resonance of the single ion is executed. This ensures single ion operation and exclude drifts of the resonance due to slow field fluctuations. During an optical double resonance measurement the frequency is set alternatingly to four discrete detunings Δ : $\Delta = 0$ kHz to measure the maximal

resonance fluorescence rate for normalization, $\Delta = 15$ kHz to ensure an unchanged center frequency, $\Delta = 250$ kHz to measure the background (not shown), and a variable detuning Δ that is different for each of these measurement cycles. A measurement cycle with a given value of Δ is repeated typically 40 times and finally data points with equal magnitude of Δ are averaged. The solid line represents the result of a Lorentzian fit. The data on the right-hand side of figure 5 is taken under the same experimental conditions, however an additional field with $\partial_z B_1 \neq 0$ is applied. The line profile is substantially altered, showing a sideband structure at the axial trap frequency that is determined independently by parametric heating to 46.0(5) kHz. A fit of this spectrum by a sum of two Lorentzians yields $a_s/a_0 = 0.084(8)$.

From this ratio, $\langle n \rangle = 6.9(6) \cdot 10^4$ – corresponding to a temperature $T = 306(30)$ mK – is deduced using equation (9) with η_{eff} independently extracted from the addressing measurements presented above. This temperature is substantially higher than the Doppler temperature for Yb ions ($T_D = 471 \mu\text{K}$). It is due to the delay time of 50 ms between cooling the ion and performing the measurements, and the low cooling efficiency during the measurement itself. For the measurement presented here demonstrating for the first time the coupling between spin and motional states in a magnetic

field gradient a higher temperature is advantageous, since it increases the relative height of the motional sideband.

In conclusion, we have demonstrated the addressing in frequency space of individual spins that are part of a Coulomb crystal formed by atomic ions confined in an electrodynamic cage. We also proved experimentally the coupling between spin states and motional states – described by an effective Lamb-Dicke parameter – when the ions are exposed to a magnetic field gradient. These are two fundamental experimental steps undertaken on the way towards realizing a novel physical system for quantum information science, an ion spin molecule. To make full use of the advantages this system offers, substantially higher magnetic field gradients have to be applied in the future. This will be possible when employing, for instance, miniaturized ion traps that are under development and will allow for gradients of about > 100 T/m. This will allow to distinguish several tens of ions in frequency space with negligible cross-talk, and will induce a large effective Lamb-Dicke parameter and thus spin-spin coupling constants.

We thank Christian Schneider for support in operating the experiment. Financial support by Deutsche Forschungsgemeinschaft and the European Union (Integrated Project Qubit Applications) is acknowledged.

-
- [1] R. P. Feynman, *Int. J. Theor. Phys.* **21**, 467 (1982).
 [2] S. Lloyd, *Science* **273**, 1073 (1996).
 [3] D. Porras and J. I. Cirac, *Phys. Rev. Lett.* **93**, 263602 (2004).
 [4] A. Aspuru-Guzik, A. D. Dutoi, P. J. Love, and M. Head-Gordon, *Science* **309**, 1704 (2005).
 [5] W. Dür and H.-J. Briegel, *Phys. Rev. Lett.* **92**, 180403 (2004).
 [6] A. R. R. Carvalho, F. Mintert, and A. Buchleitner, *Phys. Rev. Lett.* **93**, 230501 (2004).
 [7] P. Zoller, T. Beth, D. Binosi, R. Blatt, H. Briegel, D. Bruss, T. Calarco, J. I. Cirac, D. Deutsch, J. Eisert, et al., *The European Physical Journal D - Atomic, Molecular, Optical and Plasma Physics* **36**, 203 (2005).
 [8] F. Schmidt-Kaler, H. Häffner, M. Riebe, S. Gulde, G. P. T. Lancaster, T. Deuschle, C. Becher, C. F. Roos, J. Eschner, and R. Blatt, *Nature* **422**, 408 (2003).
 [9] D. Leibfried, B. DeMarco, V. Meyer, D. Lucas, M. Barrett, J. Britton, W. M. Itano, B. Jelenkovic, C. Langer, T. Rosenband, et al., *Nature* **422**, 412 (2003).
 [10] K.-A. Brickman, P. C. Haljan, P. J. Lee, M. Acton, L. Deslauriers, and C. Monroe, *Phys. Rev. A* **72**, 050306 (2005).
 [11] J. P. Home, M. J. McDonnell, D. M. Lucas, G. Imreh, B. C. Keitch, D. J. Szwer, N. R. Thomas, S. C. Webster, D. N. Stacey, and A. M. Steane, *New Journal of Physics* **8**, 188 (2006).
 [12] D. Kielpinski, C. Monroe, and D. J. Wineland, *Nature* **417**, 709 (2002).
 [13] T. Schulte-Herbrüggen, A. Spoerl, N. Khaneja, and S. Glaser, *arXiv:quant-ph/0502104v1* (2005).
 [14] T. Schulte-Herbrüggen, A. Spörl, and S. Glaser, *arXiv:0712.3227v1* (2007).
 [15] C. Wunderlich, *Laser Physics at the Limit* (Springer, 2002), chap. Conditional Spin Resonance with Trapped Ions, p. 261.
 [16] C. Wunderlich and C. Balzer, *Advances in Atomic, Molecular, and Optical Physics* **49**, 293 (2003).
 [17] D. M. Hugh and J. Twamley, *Phys. Rev. A* **71**, 012315 (2005).
 [18] D. J. Wineland, J. C. Bergquist, W. M. Itano, J. J. Bollinger, and C. H. Manney, *Phys. Rev. Lett.* **59**, 2935 (1987).
 [19] F. Mintert and C. Wunderlich, *Phys. Rev. Lett.* **87**, 257904 (2001).
 [20] M. Loewen, Master's thesis, Universität Hamburg (2003).
 [21] X.-L. Deng, D. Porras, and J. I. Cirac, *Phys. Rev. A* **72**, 063407 (2005).
 [22] M. Pons, V. Ahufinger, C. Wunderlich, A. Sanpera, S. Braungardt, A. Sen(De), U. Sen, and M. Lewenstein, *Phys. Rev. Lett.* **98**, 023003 (2007).
 [23] S. Braungardt, A. Sen(De), U. Sen, and M. Lewenstein, *Phys. Rev. A* **76**, 042307 (2007).
 [24] R. Raussendorf and H. J. Briegel, *Physical Review Letters* **86**, 5188 (2001).
 [25] M. Hein, W. Dür, J. Eisert, R. Raussendorf, M. V. den Nest, and H.-J. Briegel, *Proceedings of the International School of Physics "Enrico Fermi" Quantum Computers, Algorithms and Chaos Varenna, Italy* (IOS Press, Amsterdam, 2006), chap. Entanglement in graph states and its applications, p. 162.
 [26] H. Wunderlich, Master's thesis, Universität Siegen (2007).
 [27] C. Balzer, A. Braun, T. Hannemann, C. Paape, M. Ettlér, W. Neuhauser, and C. Wunderlich, *Physical Review A (Atomic, Molecular, and Optical Physics)* **73**, 041407(R) (2006).
 [28] C. Gerz, J. Roths, F. Vedel, and G. Werth, *Zeitschrift für Physik D Atoms, Molecules and Clusters* **8**, 235 (1988).
 [29] D. J. Wineland and W. M. Itano, *Phys. Rev. A* **20**, 1521 (1979).
 [30] J. I. Cirac and P. Zoller, *Phys. Rev. Lett.* **74**, 4091 (1995).
 [31] C. Monroe, D. M. Meekhof, B. E. King, W. M. Itano, and D. J. Wineland, *Phys. Rev. Lett.* **75**, 4714 (1995).